"This document is the Accepted Manuscript version of a Published Work that appeared in final form in ACS Catalysis, copyright © 2017 American Chemical Society after peer review and technical editing by the publisher. To access the final edited and published work see
http://pubs.acs.org/doi/abs/10.1021/acscatal.7b00603

Hydrogenative Carbon Dioxide Reduction Catalyzed by Mononuclear Ruthenium Polypyridyl Complexes: Discerning between Electronic and Steric Effects

Takashi Ono,[a] Shuanglin Qu,[b] Carolina Gimbert-Suriñach,[a] Michelle A. Johnson,[b] Daniel J. Marell,[b] Jordi Benet-Buchholz,[a] Christopher J. Cramer,[b,] and Antoni Llobet[a,c,*]*

[a] Institute of Chemical Research of Catalonia (ICIQ), Barcelona Institute of Science and Technology (BIST), Av. Països Catalans 16, Tarragona E-43007, Spain; E-mail: allobet@iciq.es

[b] Department of Chemistry, Chemical Theory Center, and Supercomputing Institute, University of Minnesota, 207 Pleasant St. SE, Minneapolis, MN 55455-0431 +1 (USA); E-mail: cramer@umn.edu; Twitter: @ChemProfCramer

[c] Departament de Química, Universitat Autònoma de Barcelona, Cerdanyola del Vallès, Barcelona E-08193, Spain.

Takashi Ono and Shuanglin Qu contributed equally

Abstract

The preparation and isolation of a family of Ru-Cl complexes containing the deprotonated anionic tridentate meridional ligand (1Z,3Z)-N^1,N^3-di(pyridin-2-yl)isoindoline-1,3-diimine (H*bid*) and 1,3-di(2-pyridyl)benzene) (H*dpb*) namely, [Ru(bid)(acac)Cl], **1d**, [Ru(bid)(6,6'-Me_2-bpy)Cl], **1e**, *trans*-[Ru(bid)$(py)_2$Cl], **2**, [Ru(dpb)(bpy)Cl], **3a**, and [Ru(dpb)(4,4'-$(COOEt)_2$-bpy)Cl], **3b** is reported. All these complexes have been thoroughly characterized in solution by NMR spectroscopy and for **1d** and **1e** by single crystal X-ray diffraction analysis. Furthermore, the redox properties of all complexes have been investigated using cyclic voltammetry (CV) and differential pulse voltammetry (DPV). The capacity of the various complexes to catalyze hydrogenative CO_2 reduction was also investigated. Compound **1e** is the best catalyst, achieving initial turnover frequencies above 1000 h^{-1}. Kinetic analysis identifies a relationship between Ru(III/II) couple redox potentials and initial turnover frequencies. Finally, DFT calculations further characterize the catalytic cycle of these complexes and rationalize electronic and steric effects deriving from the auxiliary ligands.

KEYWORDS: catalytic carbon dioxide reduction, catalytic carbon dioxide hydrogenation, ruthenium polypyridyl complexes, transition metal redox properties, DFT.

1. Introduction

Carbon dioxide (CO_2) is the planet's primary greenhouse gas and its atmospheric concentration has been rapidly rising in the last decades due to an increased utilization of fossil fuels, resulting in global warming.[1-4] In this context, the use of abundant, cheap and non-toxic CO_2 gas as a carbon feedstock to produce liquid or gaseous fuels is an appealing solution for a carbon neutral energy scheme that would help to palliate these harmful environmental consequences. The CO_2 molecule is thermodynamically stable and kinetically inert and its transformation to useful materials remains an important challenge for the research community. Another issue associated with CO_2 is the selectivity of its conversion to higher-value reduced products given the myriad of derivatives that can be obtained, depending on the degree of reduction of the molecule. Reduction can proceed from two-electron products such as carbon monoxide and formic acid to more useful products such as methanol or all the way to eight-electron reduced methane. One approach to overcome the kinetic barrier and selectivity challenge of the CO_2 reduction reaction is the use of transition metal complexes as catalysts.[5-8] They have been successfully used under electrochemical,[5, 9] photochemical[6,8, 10-12] and chemical conditions.[7, 13] One promising chemical strategy is the selective reduction of CO_2 with hydrogen gas to formic acid.[7, 13-27] The reverse reaction, that is, the transformation of formic acid/formate ion into CO_2 and H_2 gases is thermodynamically favored, and thus formic acid has been recognized as a hydrogen storage material with high atom-efficiency when suitable catalysts are used.[28-29,24-25, 30-33]

For all these reasons significant efforts have recently been devoted to the development of new and more efficient transition metal complexes that can catalyze the hydrogenative reduction of CO_2 with the objective of reaching high turnover numbers and high selectivity under milder conditions.[7] An additional challenge in this field is the discovery of catalysts

sufficiently active to react with today's atmospheric CO_2 concentrations, which are in the micromolar range, thereby potentially decreasing significantly its impact as a greenhouse gas.[34]

A fundamental aspect that needs to be developed to be able to succeed in this endeavor is to understand and master the factors governing catalyst reactivity. It is imperative to unravel alternative mechanistic pathways that operate at a molecular level in the hydrogenative reaction as well as deactivation pathways linked to the catalytic cycle, in order to optimize the former and suppress the latter. Efforts along these lines have been recently reported by Himeda and Fujita, who have developed a family of iridium complexes containing bipyridine or phenanthroline ligands with electron-donating substituents, as well as with the presence of proton responsive functionalities. [7, 16-17, 23-25] These experiments have made clear the impact of electronic effects on catalyst efficiency for this particular system. Additionally, recent DFT studies by the group of Neese et al. have shed light on the controversial effects of metal hydricity as it impacts the overall performance of Fe and Co complexes that had previously been shown to be active for hydrogenative CO_2 reduction.[18-19, 21-22]

Along similar lines, we have also previously carried out a kinetic analysis of hydrogenative CO_2 reduction catalyzed by a family of mononuclear $Ru^{II}Cl$ precursor complexes containing a tridentate ligand such as 2,2':2",6'-terpyridine (*trpy*) or (1*Z*,3*Z*)-1,3-bis(pyridin-2-ylimino)isoindolin-2-ide, (bid^-) and a bidentate ligand such as 2,2'-bipyridine (*bpy*) and related substituted *bpy* ligands or 3,5-bis(2-pyridyl)pyrazolate (bpp).[14-15] These complexes are labeled **1a-c**, $\mathbf{4}^+$, ***out*-5**$^+$ and ***in*-5**$^+$ and drawn structures are presented in Chart 1.

In this work we have extended this family to new mononuclear $Ru^{II}Cl$ precursor complexes containing the bid^- ligand with additional auxiliary ligands completing the

octahedral coordination sphere of the Ru center including [Ru(bid)(acac)Cl], **1e**, and *trans*-[Ru(bid)(py)$_2$Cl], **2**. In addition we have also prepared complexes containing the anionic ligand 1,3-di(2-pyridyl)benzene (H*dpb*) with bpy and 4,4'-(COOEt)$_2$-bpy, [Ru(dpb)(bpy)Cl], **3a**, and [Ru(dpb)(4,4'-(COOEt)$_2$-bpy)Cl], **3b**, and one Ru^{III} precursor **1d**, [Ru(bid)(6,6'-Me$_2$-bpy)Cl], whose structures are drawn in Chart 1.

We have evaluated the activities of these new complexes for the catalytic hydrogenation of CO_2 and we compare their performance to related complexes previously reported in the literature. Through this comparison, we rationalize the electronic and steric factors that influence the performance of our catalysts.

2. Results and Discussion:

2.1 Synthesis

The synthesis of complexes **1d-e** and **2** containing the *bid*$^-$ ligand follows a 'one-pot' procedure similar to that for complexes **1a-c.** The synthetic intermediate [Ru(Hbid)Cl$_3$] is treated with the corresponding bidentate ligand in the presence of NEt$_3$ using EtOH as solvent. On other hand complexes **3a-b** containing the *dpb*$^-$ ligand are synthesized in two steps via the formation of the cyclometalated complex *trans*-[Ru(dpb)(dmso-*s*)$_2$Cl], **6,** as a synthetic intermediate that is obtained in 79 % yield by refluxing a mixture of [RuCl$_2$(dmso)$_4$] and *Hdpb* in the presence of NEt$_3$. Addition of 4,4'-R$_2$-*bpy* (R = H, COOEt) to **6**, followed by light irradiation generates the desired Ru-Cl complexes **3a-b**, which are purified by column chromatography (see Equation 1 and the Supporting Information for additional details).

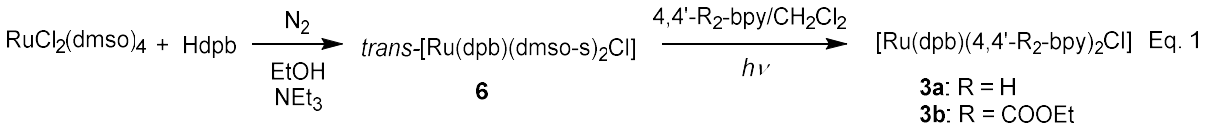

2.2 Structure

Structural characterization of **1d-e**, **2** and **3a-b** was carried out in solution by ^{1}H-NMR spectroscopy and in the solid state for **1d** and **1e** based on single crystal X-ray diffraction analysis.

Ortep plots for **1d** and **1e** are presented in Figure 1, while selected metric parameters are shown in Table 1 (**1e**, entry 1) and in the Supporting Information. In both cases **1d** and **1e** adopt an octahedral type of geometry with the typical bonding distances expected for a d^6 Ru(II) and d^5 Ru(III) complex respectively.[14-15, 35] An interesting feature related to complex **1e** is the significant distortion of the octahedral geometry due to the pronounced steric effect exerted by the methyl groups at the 6 position of the *bpy* ligand. Distortions are apparent in the relative angles of the isoindole ligand with respect to the *bpy* ligand. For an ideal octahedral geometry the dihedral angles between the planes defined by the aromatic rings of those two ligands would be 90°, but instead a value of 58.4° is found when taking the best fit for the ligand planes. The dihedral angle between the two pyridyl groups of the *bid*$^{-}$ ligand also provide some indication of the degree of distortion. For an ideal octahedral geometry the pyridyl rings would be expected to be coplanar, i.e., to have a 0° dihedral angle, but in **1e** a value of 34.7° is found for this angle. Finally, the Ru-N bonds to the Me_2-bpy ligand are about 0.06 Å longer in **1e** compared to the less sterically encumbered **1a**.[15]

NMR spectroscopic characterization for the newly synthesized complexes is presented in the Supporting Information (Figures S1-5), and in Figure 2 for complex **2**. The ^{1}H NMR spectrum of **2** shows only one set of coordinated pyridine resonances, clearly indicating their *trans* disposition. The larger thermodynamic stability of the *trans*-**2** isomer compared to *cis*-

2 derives from twice the hydrogen bonding interactions with the chlorido ligand in the former together with a favorable *trans* arrangement of the Ru-N^{-} and Ru-Cl bonds.

The interactions of the chlorido ligand with the protons of nearby pyridine ligands differ significantly in **1**-**4** depending on the relative positions of the various groups in the complexes, as expected. For instance, the protons at the 6-position of the two pyridyl rings of *bid*$^{-}$ ligand in **2** show a significant interaction as shown by a strongly deshielded doublet (δ_H 10.76 ppm vs 7.5-7.6 ppm for **1a-c**, Figure 2).[15] In contrast, this effect is not observed for the protons at the C(2)/C(6) positions of the monodentate pyridines of **2** (δ_H 7.78), likely owing to the rapid rotation of these ligands on the NMR time scale. However, deshielding is observed for **1a-c**[15] and **4**$^{+}$[36] as well as **3a-b** (δ_H 10.29 for **3a** and 10.43 for **3b**, respectively) due to the close proximity of the chlorido ligand to the C(6) proton of one of the pyridyl rings of the *bpy* ligand. Similarly, for the sterically hindered compound **1e**, the ^{1}H NMR spectrum shows that one of the methyl groups substituting the *bpy* ligand appears at lower field (δ_H: 3.32 ppm, vs 1.41 ppm for the other methyl group) as a consequence of the deshielding effect of the adjacent chlorido group (Figure S1).

2.3 Redox properties

The electrochemical properties of complexes **1-5** were examined by means of cyclic voltammetry in dichloromethane and the observed redox potentials for the Ru(III/II) couple are collected in Table 2.

The $E_{1/2}$ values (vs SSCE) for the Ru(III/II) couple for *bid*$^-$/*bpy* systems **1a-c**, **e** are in the range of 0.17 to 0.41 V, varying with electron donating/withdrawing groups on the *bpy* ligand, and are shifted 460-700 mV cathodically compared to that of *trpy* analogue **4**$^+$ ($E_{1/2}$ = 0.87 V). These shifts are ascribed to the additional electron density on the metal center supplied by the anionic character of *bid*$^-$ ligand.

Interestingly, electron donating Me groups at the 6,6'-positions of *bpy* do not alter the $E_{1/2}$ value with respect to **1a** (0.30 V for both **1a** and **1e**). This is in contrast to that for the related trpy complex which contains Me groups at the 4,4'-positions of *bpy*: the $E_{1/2}$ for [Ru(trpy)(4,4'-Me_2-bpy)Cl]$^+$ (0.79 V vs. Ag/AgCl in CH_3CN) is 50 mV lower than that for [Ru(trpy)(bpy)Cl]$^+$ (0.84 V vs. Ag/AgCl in CH_3CN).[37] On the other hand, a similar trend has been found for the sterically demanding ligand 2,9-Me_2-phen (phen = 1,10-phenanthroline) in [Ru(trpy)(2,9-Me_2-phen)Cl]$^+$ whose $E_{1/2}$ value (0.83 V vs SSCE in CH_3CN) is 20 mV *higher* than that for non-substituted [Ru(trpy)(phen)Cl]$^+$ (0.81 V vs SSCE in CH_3CN).[38] We thus conclude that the increased electron donation that would otherwise be associated with methyl substitution is mitigated by the strongly distorted geometry induced by the Me substituents (see X-ray structure of **1e** in Figure 1). The replacement of the *bpy* ligand with the strongly σ-donating anionic *acac*$^-$ ligand decreases its redox potential by nearly 800 mV compared to compounds **1a**–**c** and **2**.

The incorporation of the metal-carbon σ-bond in **3a** also results in a large cathodic shift of the Ru(III/II) couple ($E_{1/2}$ = 0.02 V; $E_{p,a}$ = 0.074, $E_{p,c}$ = -0.036 V), i.e., more than ***800***

mV with regard to *trpy* analogue **4**$^{+}$**.** Remarkably, in **3a** we can also observe a chemically and electrochemically reversible wave for the IV/III couple ($E_{1/2}$ = 1.39 V; $E_{p,a}$ = 1.449, $E_{p,c}$ = 1.330 V, $\Delta E = E_{1/2}$(IV/III)-$E_{1/2}$(III/II) = 1.37 V) as can be seen in Figure 3. The latter is only 100 mV anodically shifted compared to the III/II couple for $Ru(bpy)_3^{2+}$ or $Ru(trpy)_2^{2+}$ ($E_{1/2}$ = 1.28 V in CH_3CN for both).[39] This huge cathodic shift is also observed in related complexes: $E_{1/2}$ = 0.51 V for $[Ru(dpb)(trpy)]^+$ in CH_3CN.[39] This is a striking example of how the electron density around a metal center can be manipulated by ligand substitution with electron donating or withdrawing groups.

Complexes *out*-**5**$^{+}$ and *in*-**5**$^{+}$, containing pyrazolylic protons from the *bpp* ligand, can be deprotonated under the basic conditions used for the catalytic reaction and this speciation is reflected in the oxidation potentials of the different forms (Figure S10 in the Supporting Information). The $E_{1/2}$ values for the protonated forms are 0.63 and 0.82 V, close to that of **4**$^{+}$, while deprotonation results in significantly lowered $E_{1/2}$ values (0.30 and 0.43 V) due to the negative charge of the *bpp*$^{-}$ ligand. This significant shift in the potential could potentially alter their catalytic performance compared to **4**$^{+}$.

2.4 Catalytic Experiments

Complexes **1d-e**, **2**, **3a-b**, *out*-**5**$^{+}$, and *in*-**5**$^{+}$ were tested as catalyst precursors for the hydrogenative reduction of CO_2 in 2,2,2-trifluoroethanol as solvent with added NEt_3 to form formate (and triethyl ammonium counterion) as the sole product, in analogy to previous results reported for **1a-c** and **4**$^{+}$.[15] Figure 4 reports the time profiles for the generation of HCOOH for all of the complexes and their catalytic activities are reported in Table 2 in terms of initial turnover frequencies (TOF_i) measured over the first 90 minutes. For complex **1e**, the TOF_i was obtained considering instead only the first 20 minutes owing to the much faster

reactivity of this complex compared to the others (TOF_i > 1140 h^{-1} for **1e** *vs* 366 h^{-1} for **1a**, see Figure 4).

Comparing the effect of the stronger σ-donating *dpb*$^-$ ligand with the *bid*$^-$ ligand, **3a** showed lower catalytic activity (TOF_i: 192.6 h^{-1}) than that of *bid*$^-$ analogue **1a** (TOF_i: 366 h^{-1}). Complex **3b** containing electron withdrawing groups (-CO_2Et) on the *bpy* ligand showed higher activity than **3a**, a trend that was also found for the *bid*$^-$ family of complexes (**1a-b**).[15] In contrast, a series of *trpy* complexes showed opposite results regarding electron-donating abilities, that is, the replacement of neutral *bpy* by anionic *bpp*$^-$ formed by *in-situ* deprotonation from complexes *in*-**5**$^+$ and *out*-**5**$^+$ resulted in 37 and 72 times higher catalytic activity than that of *bpy* analogue **4**$^+$ (entries 9-11 in Table 2).

Complex **2**, which unlike all others has a reactive site *trans* to the center ring of the tridentate ligand, showed lower catalytic activity compared to the rest of the active *bid*$^-$ family of complexes **1a-c**, **e** (compare entry 6 with entries 1-3, 5 in Table 2). Interestingly, complex **1d**, which has the lowest $E_{1/2}$ value (-0.49 V) in this study thanks to its bidentate anionic *acac*$^-$ ligand, exhibited no activity.

Figure 5 summarizes the different trends observed for the catalytic systems by showing a relationship between TOF_i and $E_{1/2}$ for the Ru(III/II) couple of the catalysts studied here. Figure 5 clearly shows that for the complexes having anionic tridentate ligands (*bid*$^-$ or *dpb*$^-$), TOF_i increases with an increase in the redox potential. By contrast, complexes having neutral *trpy* ligand show opposite results, i.e., TOF_i increases with a *decrease* of $E_{1/2}$. The different behaviors of **1a**, **1e**, and **2** are also striking, given that they have very similar $E_{1/2}$ values but radically different TOF_i. In order to further illuminate the origin of these apparently contradictory trends and gain a more complete understanding of the overall reduction mechanisms, we turned to DFT calculations as discussed in the next section.

2.5 Mechanistic Proposal and DFT Calculations

We have earlier described key steps in a mechanism for mononuclear *bid*$^-$ complexes (**1a**-**1c**) that rationalized the effect of electron-donating and electron-withdrawing groups on catalyst performance.[15] To gain further insight into ligand electronic and steric effects operative for the new catalysts reported here, we performed calculations for all of the complexes **1-5** (except **1b** and **1c**, whose comparison to **1a** was reported previously, as noted). A complete reaction scheme for the catalytic process is summarized in Scheme 1, which includes both initiation and the complete catalytic cycle. First, chloride dissociates from the pre-catalyst to permit binding of H_2. This is followed by heterolytic cleavage of the H-H bond, leading to the active Ru-H species (blue portion of Scheme 1). Subsequently, nucleophilic attack of the hydride on CO_2 generates a transient Ru-HCOO intermediate, which can isomerize to the more stable metal formate Ru-OCHO.[40-41] Dissociation of formate then permits binding of another equivalent of H_2 (black portion of scheme). [Included in gray in the scheme is a path recognizing the potential for liberated formate to serve as the base that deprotonates the Ru-H_2 intermediate. As detailed in the supporting information (SI), standard-state activation free energies computed for TS-H_2(O) are usually a bit lower than those computed for TS-H_2(N), i.e., formate is indeed a slightly stronger base than trimethylamine (used for computation) when both are present at the same concentration. However, the vast excess of amine present compared to formate in the experimental system, particularly at the low conversions where the kinetics are measured, dictates that the rates for amine acting as base will be higher than those for formate acting as base, and we restrict further discussion below to paths involving TS-H_2(N).] For the case of compounds *out*- and *in*-**5**, the catalytic cycle in Scheme 1 effectively "doubles" in possible scope, as every

intermediate may exist in a conjugate acid or base form associated with the protonation state of the pyrazole ligand, as described in more detail below.

Free energy diagrams of the catalytic cycle for selected compounds of **1**-**5**, taking the Ru-H intermediate as the relative zero of energy within each system to facilitate comparison, are shown in Figure 6; ball-and-stick transition-state (TS) structures for **1e** are also shown and are representative for the other systems as well with respect to the qualitative geometries of the reacting species about the metal center. The predicted energies of species and TSs of the catalytic cycle for *all* complexes studied are summarized in Table 3 (results of the catalyst initiation process are giving in Table S2 in SI). As the predicted relative free energy of TS-H_2(N) is higher than that of TS-H in every instance, DFT predicts the heterolytic cleavage of H_2 to be the turnover-limiting step for all compounds (the two free energies are close for **2**, but as the activation free energy from resting Ru-OCHO to TS-H of the next cycle would involve the difference in their free energies reduced by the favorable driving force of the reaction, heterolytic cleavage remains turnover-limiting). To understand ligand effects on relative rates, this then suggests that we should focus on the degree to which they stabilize or destabilize the Ru-OCHO intermediates and TS-H_2(N), noting that either destabilizing Ru-OCHO or stabilizing TS-H_2(N) will improve activity.

We first consider the *bid*$^-$ containing complexes, which show increased TOF_i with increasing $E_{1/2}$ of the Ru(III/II) couple, i.e., with addition of electron withdrawing substituents on the *bpy* ligand. The anionic *bid*$^-$ ligand has a high capacity for sigma donation of electron density to the metal center, producing initial complexes that have high thermodynamic hydricity (low ΔG^o_{H-})[42-45] and thus react readily with CO_2, so that this step is not turnover limiting. Instead, the H-H cleavage step with its associated $\Delta G_2^{\circ,\ddagger}$ is turnover

limiting. The acidity of coordinated H_2 *increases* when electron-withdrawing substituents are present on the *bid*$^-$ ligand, reducing the activation free energy for this step, consistent with experimental trends shown in Figure 5 (**1a**, **1b**, **1c**) and discussed already in our previous study. Let us now compare **1a** with **1d**, **1e**, and **2**.

Replacing the neutral *bpy* ligand of **1a** with the anionic *acac* ligand makes **1d** a Ru^{III} complex. The hydricity of the Ru-H intermediate for **1d** is significantly lower than observed for the Ru^{II} complexes, as quantified by an activation free energy for hydride transfer ($\Delta G_1^{\circ,\ddagger}$) that is higher than that for **1a** by 3.4 kcal/mol (cf. Figure 6 and Table 3). Still more notably, it is much more difficult to dissociate the formato ligand from the Ru-OCHO intermediate for **1d** compared to **1a** (this is true for dissociation of chloride from Ru-Cl as well, see SI). Comparing **1d** to **1a**, the energy costs to dissociate formate are 19.1 and 11.9 kcal mol^{-1}, respectively. This contributes to an activation free energy for H_2 heterolysis in **1d** of 26.2 kcal mol^{-1}, which is the highest such $\Delta G_2^{\circ,\ddagger}$ value of any compound studied here and consistent with **1d** exhibiting no experimental catalytic activity (entry 4, Table 2).

Considering next **1a**, **1e**, and **2**, these three compounds all have similar $E_{1/2}$ values. Consistent with that observation, all three are predicted to have very similar values for $\Delta G_1^{\circ,\ddagger}$, although that step is not turnover-limiting (Figure 6 and Table 3). Nevertheless, they exhibit significantly different TOF_i values, suggesting that strong differences must be manifest in $\Delta G_2^{\circ,\ddagger}$ values, and that is indeed computed to be the case. In the case of **1e**, the methyl groups at the 6 and 6′ positions of the *bpy* ligand introduce significant steric bulk that distorts the ligand framework about Ru (Figures 1 and 7) and destabilizes the bound formato ligand relative to other stationary points having smaller ligands at the reactive metal site (Figure 6). This reduces $\Delta G_2^{\circ,\ddagger}$ for **1e** to 18.9 kcal mol^{-1} compared to 20.1 kcal mol^{-1} for **1a** (a somewhat

greater reduction is predicted for initiation, see Table S1 of supporting information). This agrees with the 3-fold faster rate for CO_2 reduction measured for **1e** compared to **1a** (entries 1 and 5 in Table 2).

Considering next complex **2**, the replacement of *bpy* in either **1a** or **1e** with two pyridine ligands oriented *trans* to one another doesn't significantly influence the reduction potential, but it *does* permit a relatively unstrained octahedral arrangement of the ligands about Ru and moreover the individual pyridine ligands each twist so as not to crowd the open metal coordination site with their ring edges. This significantly stabilizes the bulkier Ru-OCHO intermediate relative to other stationary points, so that for **2** it is 3.6 kcal mol^{-1} more stable relative to Ru-H than is the case for **1a** (Figure 6 and Table 3). The more open coordination site also stabilizes TS-H_2(N) relative to Ru-H, but to a lesser degree than for Ru-OCHO, such that $\Delta G_2^{\circ,\ddagger}$ for **2** is higher than that for **1a** by 2.7 kcal/mol, again in qualitative agreement with the experimental TOF_i for the former being about three times smaller than that for the latter (Entries 1 and 6 in Table 2).

For the complexes containing the anionic *dpb*$^-$ ligands (**3a** and **3b**), an increase in reactivity is observed with increasing $E_{1/2}$ (*bpy* of **3a** vs 4,4'-$(COOEt)_2$-*bpy* of **3b**). The analysis previously reported[15] for **1a** and **1b** should apply analogously to **3a** and **3b**. However, the increase in activity for **3a** compared to **3b** is quite small, and computation simply predicts **1a**, **3a**, and **3b** to have turnover-limiting activation free energies all within one kcal mol^{-1} of one another (Table 3 and Figure S12) which cannot be reliably further interpreted within the expected error of our DFT model.

The replacement of the *bid*$^-$ ligand in **1a** with the neutral *trpy* ligand makes catalyst $\mathbf{4}^+$ positively charged. As expected, this reduces the hydricity of the relevant Ru-H

intermediate when compared to compounds **1**-**3** (Table 3 and Figure 6). Furthermore, this positive charge makes it much more energetically costly to dissociate the formato ligand from Ru-OCHO (uphill by 18.3 kcal mol^{-1}), so that the overall activation free energy $\Delta G_2^{\circ,\ddagger}$ is 24.6 kcal/mol, which is the second highest value for this quantity reported in Table 3 and consistent with the almost complete lack of catalytic activity for **4**$^+$ observed experimentally.

Turning finally to complexes *in*-**5**$^+$ and *out*-**5**$^+$, as noted above, the pyrazole protons of the *bpp* ligand can be deprotonated under suitably basic conditions, which might be expected to lead to catalytic performances different from that exhibited by **4**$^+$; theory indeed predicts that to be the case. Dissociation of chloride (initiation) or formate (turnover) from either **5**$^+$ compound to generate dicationic intermediates is predicted to be quite energetically costly. The deprotonated, monocationic conjugate base forms—corresponding to Ru$^+$, Ru$^+$-H_2, and TS-H_2(N)—are, by contrast, predicted to be 7-10 kcal mol^{-1} more stable, and it is their energies that are included in Table 3. All of the other stationary points are predicted to have lower standard-state free energies for their conjugate acid forms. In some instances, the energetic separation is small, however, suggesting that both conjugate acid and base forms may have non-negligible concentrations in the presence of excess base. Full reaction coordinate diagrams for initiation and propagation of *in*- and *out*-**5**$^+$ are provided in Figures S13-S18. The somewhat reduced activity of *in*-**5**$^+$ compared to *out*-**5**$^+$ appears to be related to the *trans* effect of the strong-field pyridine donor present in the former compared to the latter (see Figure S19). This reduces the pK_a of every stationary point of *in*-**5**$^+$ compared to *out*-**5**$^+$, and as the turnover-limiting activation free energy is associated with the conjugate *base* form of TS-H_2(N) and the conjugate *acid* form of Ru-OCHO, this variation in pK_a increases $\Delta G_2^{\circ,\ddagger}$ from 20.6 kcal mol^{-1} for *out*-**5**$^+$ to 22.2 kcal mol^{-1} for *in*-**5**$^+$.

The computational analysis above does not capture perfectly all trends associated with significant variations in ligands. Nevertheless, considering all of the data in Table 3, if the relative free energies of activation for the predicted turnover limiting step ($\Delta G_2^{\circ,\ddagger}$) are correlated against corresponding $-RT$ ln(TOF_i) values from Table 2, the resulting Pearson correlation coefficient is $R = 0.884$ — a quite reasonable correlation given the wide variety of ligands and charge states studied. Another key feature of the computational analysis is that, just as we found originally when considering a smaller range of substrates,[15] in all of these cases the turnover-limiting step continues to be deprotonation of the Ru-H_2 intermediate; in no case is the hydricity of the Ru-H intermediate so low as to make nucleophilic attack on CO_2 turnover-limiting.

3. Conclusions

We have studied a family of mononuclear Ru complexes as catalysts for hydrogenative CO_2 reduction focusing on the effects of variations in the electronic and steric properties of the corresponding ligands. Kinetic analysis of the reaction reveals a relationship between TOF_i values and redox potentials for the Ru(III/II) couple of the corresponding Ru-Cl complexes (Figure 5) that is consistent with the turnover-limiting step for strongly sigma-donating ligands *bid*$^-$ and *dpb*$^-$ being heterolysis of Ru-bound H_2 (H-H cleavage in Scheme 1and Figure 6). Moreover, density functional studies predict this step to be turnover-limiting for all of the compounds examined here, suggesting that ligand modifications that destabilize the intermediate Ru-OCHO formato complex or stabilize the transition-state structure for H-H cleavage (TS-H_2) should improve catalyst activity.

The introduction of methyl substituents at the 6,6'-positions of a coordinating *bpy* ligand significantly distorts the geometry around the metal center, and a maximum TOF_i of 1140 h^{-1} has been obtained for this sterically hindered complex **1e**, which may be compared to 366 h^{-1} for analogous complex **1a**. The high activity of the former derives from the combination of the strong sigma-donation of the *bid*$^-$ ligand (ensuring that reduction of CO_2 by the metal hydride intermediate is not turnover limiting), and the steric destabilization of the subsequent Ru-OCHO intermediate that reduces the activation free energy for H_2 to replace the formato ligand and undergo heterolysis to complete the catalytic cycle. Other ligand variations reported here, including the use of ligands able to participate in conjugate acid or base forms, led to trends in TOF_i also readily rationalized based on consideration of the relative free energies of the Ru-OCHO formato intermediate and the H_2 heterolysis transition-state structure, and further efforts to tune this step should be fruitful.

Acknowledgments

Support was received from MINECO and FEDER (CTQ2015-73028-EXP, CTQ2016-80058-R) and the U.S. National Science Foundation (CHE-1361595). T.O. thanks MINECO for a pre-doctoral grant. We also acknowledge the Minnesota Supercomputing Institute (MSI) at the University of Minnesota for providing resources that contributed to the research results reported within this paper.

Supporting Information

The Supporting Information is available free of charge on the ACS Publications website at DOI: XXXXXXX/XXXXXXXXXXX.

Experimental section including general methods, synthesis, spectroscopic and electrochemical characterization of compounds **1d**, **1e**, **2**, **6**, **3a** and **3b**. X-ray diffraction data of **1d** and **1e**. Procedures for the carbon dioxide hydrogenation reactions and additional kinetic data. Computational details and Cartesian coordinates of intermediate species and TS of the catalytic cycle (PDF).

References

1. Karl, T. R.; Trenberth, K. E. *Science* **2003,** *302*, 1719-1723.
2. Raupach, M. R.; Marland, G.; Ciais, P.; Le Quéré, C.; Canadell, J. G.; Klepper, G.; Field, C. B. *Proc. Natl. Acad. Sci. U. S. A.* **2007,** *104*, 10288-10293.
3. Aresta, M.; Dibenedetto, A.; Angelini, A. *Chem. Rev.* **2014,** *114*, 1709-1742.
4. Thomas, J. M.; Harris, K. D. M. *Energy Environ. Sci.* **2016,** *9*, 687-708.
5. Costentin, C.; Robert, M.; Savéant, J.-M. *Acc. Chem. Res.* **2015,** *48*, 2996-3006.
6. Elgrishi, N.; Chambers, M. B.; Wang, X.; Fontecave, M. *Chem. Soc. Rev.* **2017**, *46*, 761-796.
7. Wang, W.-H.; Himeda, Y.; Muckerman, J. T.; Manbeck, G. F.; Fujita, E. *Chem. Rev.* **2015,** *115*, 12936-12973.
8. Berardi, S.; Drouet, S.; Francas, L.; Gimbert-Surinach, C.; Guttentag, M.; Richmond, C.; Stoll, T.; Llobet, A. *Chem. Soc. Rev.* **2014,** *43*, 7501-7519.
9. Costentin, C.; Robert, M.; Saveant, J.-M. *Chem. Soc. Rev.* **2013,** *42*, 2423-2436.
10. Ouyang, T.; Huang, H.-H.; Wang, J.-W.; Zhong, D.-C.; Lu, T.-B. *Angew. Chem. Int. Ed.* **2017,** *56*, 738-743.
11. Yamazaki, Y.; Takeda, H.; Ishitani, O. *J. Photochem. Photobiol., C* **2015,** *25*, 106-137.
12. Thoi, V. S.; Kornienko, N.; Margarit, C. G.; Yang, P.; Chang, C. J. *J. Am. Chem. Soc.* **2013,** *135*, 14413-14424.
13. Jessop, P. G.; Joó, F.; Tai, C.-C. *Coord. Chem. Rev.* **2004,** *248*, 2425-2442.
14. Ono, T.; Planas, N.; Miró, P.; Ertem, M. Z.; Escudero-Adán, E. C.; Benet-Buchholz, J.; Gagliardi, L.; Cramer, C. J.; Llobet, A. *ChemCatChem* **2013,** *5*, 3897-3903.
15. Planas, N.; Ono, T.; Vaquer, L.; Miro, P.; Benet-Buchholz, J.; Gagliardi, L.; Cramer, C. J.; Llobet, A. *Phys. Chem. Chem. Phys.* **2011,** *13*, 19480-19484.
16. Himeda, Y.; Onozawa-Komatsuzaki, N.; Sugihara, H.; Kasuga, K. *Organometallics* **2007,** *26*, 702-712.
17. Wang, W.-H.; Muckerman, J. T.; Fujita, E.; Himeda, Y. *ACS Catal.* **2013,** *3*, 856-860.
18. Mondal, B.; Neese, F.; Ye, S. *Inorg. Chem.* **2015,** *54*, 7192-7198.
19. Mondal, B.; Neese, F.; Ye, S. *Inorg. Chem.* **2016,** *55*, 5438-5444.
20. Tanaka, R.; Yamashita, M.; Nozaki, K. *J. Am. Chem. Soc.* **2009,** *131*, 14168-14169.
21. Ziebart, C.; Federsel, C.; Anbarasan, P.; Jackstell, R.; Baumann, W.; Spannenberg, A.; Beller, M. *J. Am. Chem. Soc.* **2012,** *134*, 20701-20704.
22. Fong, H.; Peters, J. C. *Inorg. Chem.* **2015,** *54*, 5124-5135.
23. Onishi, N.; Xu, S.; Manaka, Y.; Suna, Y.; Wang, W.-H.; Muckerman, J. T.; Fujita, E.; Himeda, Y. *Inorg. Chem.* **2015,** *54* , 5114-5123.
24. Ertem, M. Z.; Himeda, Y.; Fujita, E.; Muckerman, J. T. *ACS Catal.* **2016,** *6*, 600-609.
25. Wang, L.; Onishi, N.; Murata, K.; Hirose, T.; Muckerman, J. T.; Fujita, E.; Himeda, Y. *ChemSusChem* **2017**, 10, 1071-1075.
26. Wang, W.-H.; Hull, J. F.; Muckerman, J. T.; Fujita, E.; Himeda, Y. *Energy Environ. Sci.* **2012,** *5*, 7923-7926.
27. Rohmann, K.; Kothe, J.; Haenel, M. W.; Englert, U.; Hölscher, M.; Leitner, W. *Angew. Chem. Int. Ed.* **2016,** *55*, 8966-8969.
28. Grasemann, M.; Laurenczy, G. *Energy Environ. Sci.* **2012,** *5*, 8171-8181.

29. Mellmann, D.; Sponholz, P.; Junge, H.; Beller, M. *Chem. Soc. Rev.* **2016,** *45*, 3954-3988.

30. Wang, W.-H.; Xu, S.; Manaka, Y.; Suna, Y.; Kambayashi, H.; Muckerman, J. T.; Fujita, E.; Himeda, Y. *ChemSusChem* **2014,** *7*, 1976-1983.

31. Manaka, Y.; Wang, W.-H.; Suna, Y.; Kambayashi, H.; Muckerman, J. T.; Fujita, E.; Himeda, Y. *Cat. Sci. Technol.* **2014,** *4*, 34-37.

32. Hull, J. F.; Himeda, Y.; Wang, W.-H.; Hashiguchi, B.; Periana, R.; Szalda, D. J.; Muckerman, J. T.; Fujita, E. *Nat. Chem.* **2012,** *4*, 383-388.

33. Wang, W.-H.; Ertem, M. Z.; Xu, S.; Onishi, N.; Manaka, Y.; Suna, Y.; Kambayashi, H.; Muckerman, J. T.; Fujita, E.; Himeda, Y. *ACS Catal.* **2015,** *5*, 5496-5504.

34. www.esrl.noaa.gov/gmd/ccgg/trends/. Accessed on July19th, 2017.

35. Camerano, J. A.; Rodrigues, A.-S.; Rominger, F.; Wadepohl, H.; Gade, L. H. *J. Organom. Chem.* **2011,** *696*, 1425-1431.

36. Konno, H.; Kobayashi, A.; Sakamoto, K.; Fagalde, F.; Katz, N. E.; Saitoh, H.; Ishitani, O. *Inorg. Chim. Acta* **2000,** *299*, 155-163.

37. Yoshikawa, N.; Matsumura-Inoue, T.; Kanehisa, N.; Kai, Y.; Takashima, H.; Tsukahara, K. *Anal. Sci.* **2004,** *20*, 1639-1644.

38. Kaveevivitchai, N.; Zong, R.; Tseng, H.-W.; Chitta, R.; Thummel, R. P. *Inorg. Chem.* **2012,** *51*, 2930-2939.

39. Bomben, P. G.; Robson, K. C. D.; Sedach, P. A.; Berlinguette, C. P. *Inorg. Chem.* **2009,** *48*, 9631-9643.

40. Ramakrishnan, S.; Waldie, K. M.; Warnke, I.; De Crisci, A. G.; Batista, V. S.; Waymouth, R. M.; Chidsey, C. E. D. *Inorg. Chem.* **2016,** *55*, 1623-1632.

41. Li, J.; Liu, S.; Lu, X. *Bull. Chem. Soc. Jap.* **2016,** *89*, 905-910.

42. Matsubara, Y.; Fujita, E.; Doherty, M. D.; Muckerman, J. T.; Creutz, C. *J. Am. Chem. Soc.* **2012,** *134*, 15743-15757.

43. Muckerman, J. T.; Achord, P.; Creutz, C.; Polyansky, D. E.; Fujita, E. *Proc. Natl. Acad. Sci. U. S. A.* **2012,** *109*, 15657-15662.

44. Wiedner, E. S.; Chambers, M. B.; Pitman, C. L.; Bullock, R. M.; Miller, A. J. M.; Appel, A. M., *Chem. Rev.* **2016,** *116*, 8655-8692.

45. Pitman, C. L.; Brereton, K. R.; Miller, A. J. M. *J. Am. Chem. Soc.* **2016,** *138*, 2252-2260.

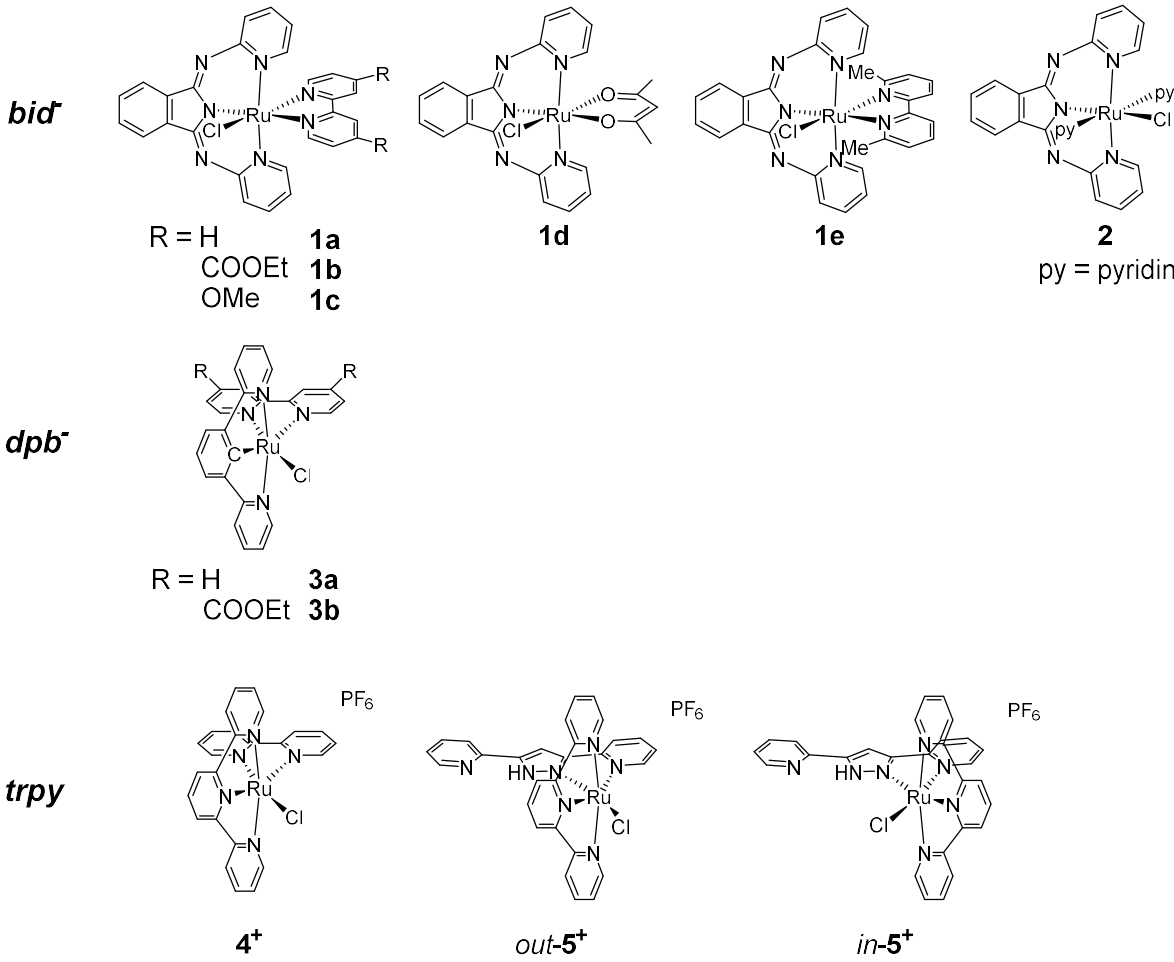

Chart 1. Studied complexes for hydrogenative CO_2 reduction.

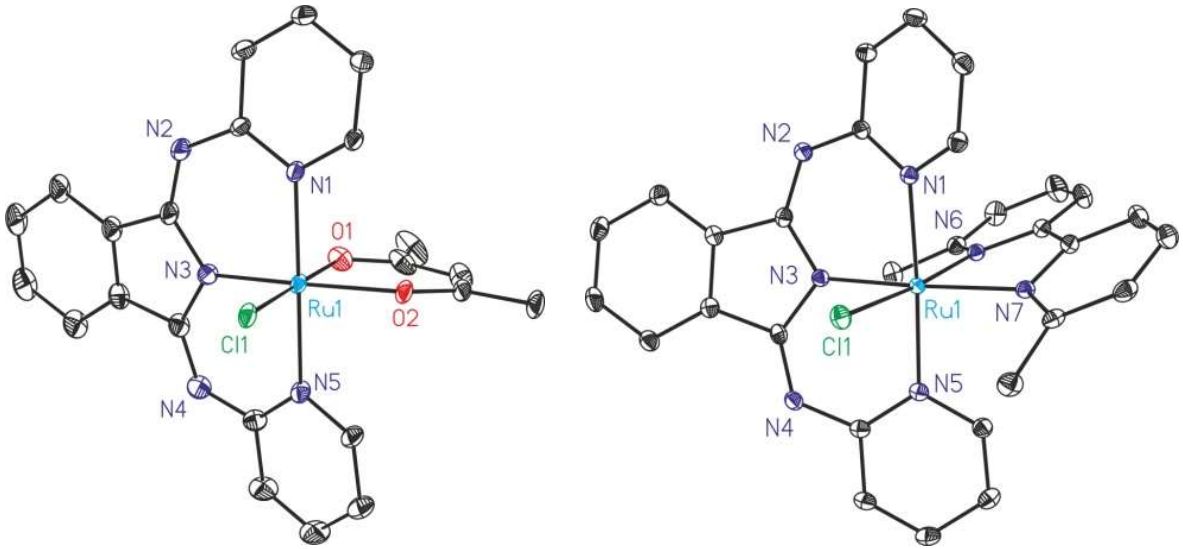

Figure 1. Ortep plots (ellipsoids at 50% probability) of the X-ray crystal structures of **1d** (Left) and **1e** (Right) together with labeling schemes. Color codes: Ru, cyan; N, blue; O, red; Cl, green; C, grey. Hydrogen atoms are not shown for clarity.

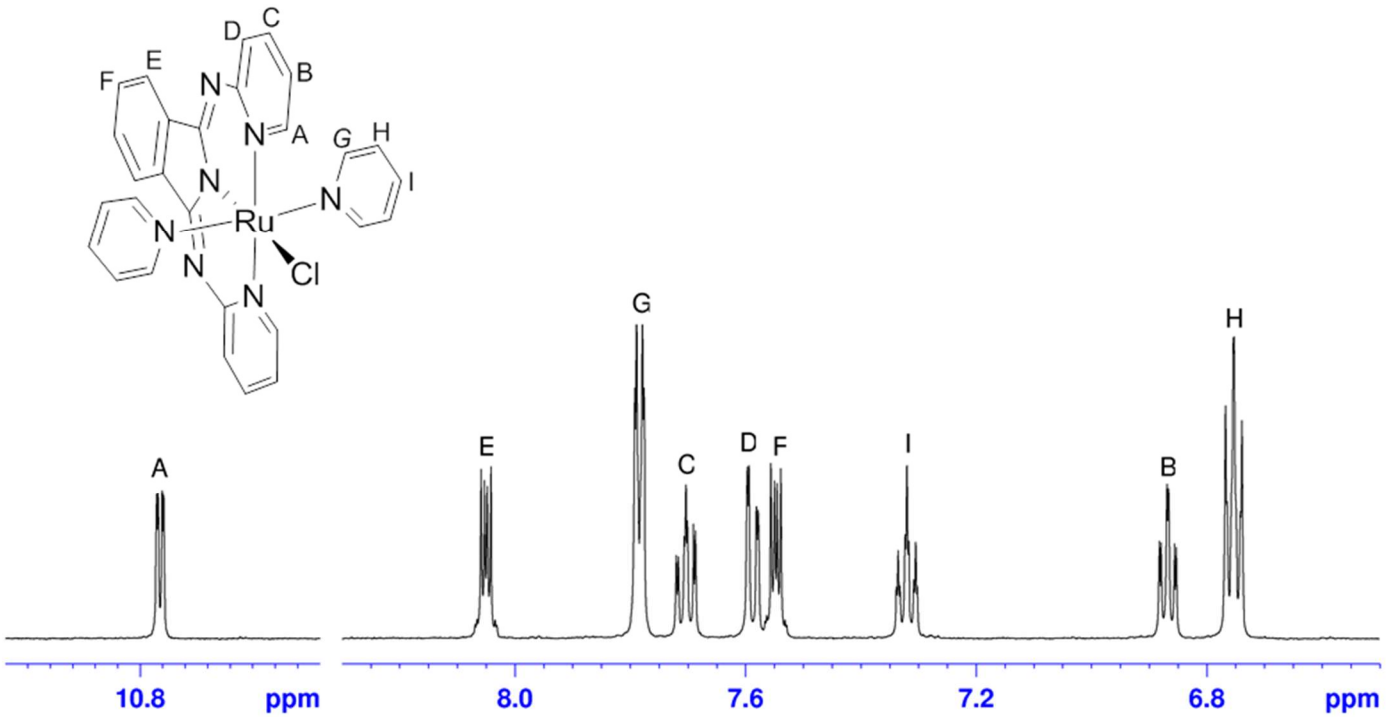

Figure 2. ^{1}H NMR spectrum of complex **2** in CD_2Cl_2 together with the labeling scheme.

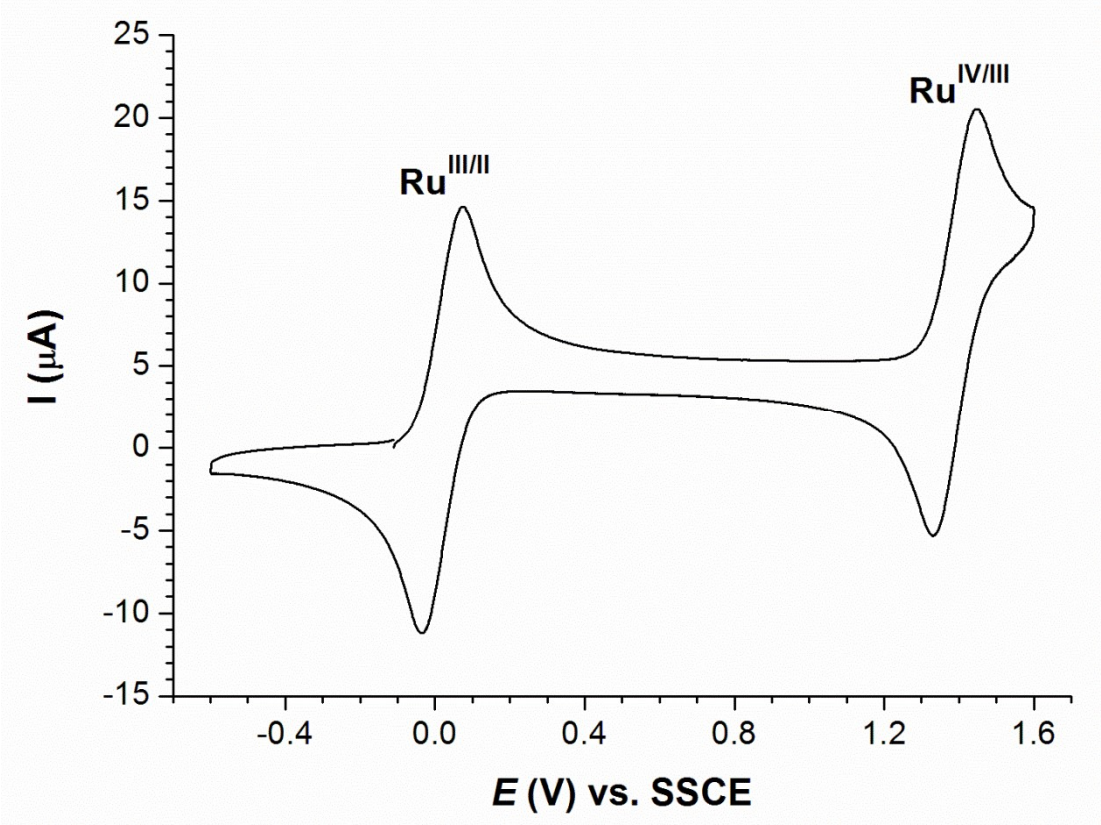

Figure 3. Cyclic voltammogram vs. SSCE at a scan rate 100 mV/s in DCM-(*n*-Bu_4N)(PF_6) (0.1 M), of complex **3a** (0.5 mM).

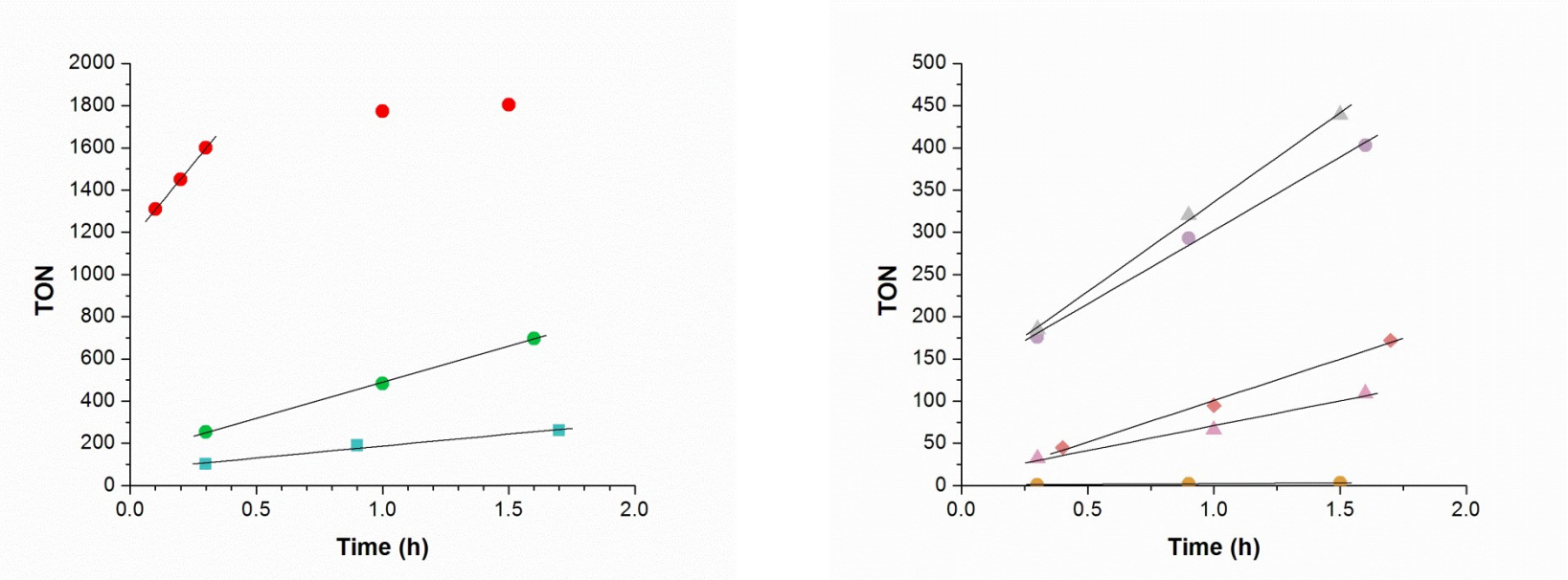

Figure 4. Initial catalytic performance of a 0.3 mM solution of Ru-Cl complex dissolved in a 9:1 mixture of TFE and NEt_3 at 25 bar of CO_2 and 25 bar of H_2 at 100 °C. Left: **1a**, ●; **1e**, ●; **2**, ■. Right: **3a**, ●; **3b**, ▲; $\mathbf{4^+}$, ●; *out*-$\mathbf{5^+}$, ◆; *in*-$\mathbf{5^+}$, ▲.

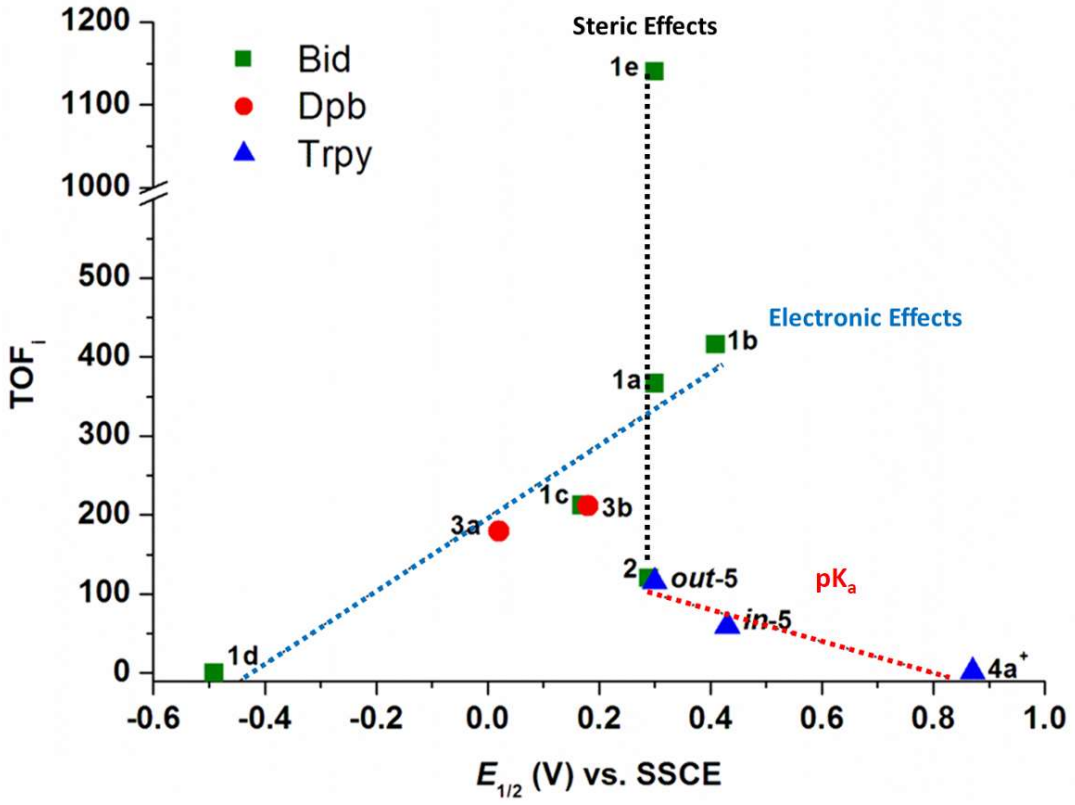

Figure 5. Plot of TOF_i with respect to $E_{1/2}$ for Ru(III/II) couple of complexes containing: *bid*$^-$ (■), *dpb*$^-$ (●), and *trpy* (▲) ligands with corresponding labeling of the complexes.

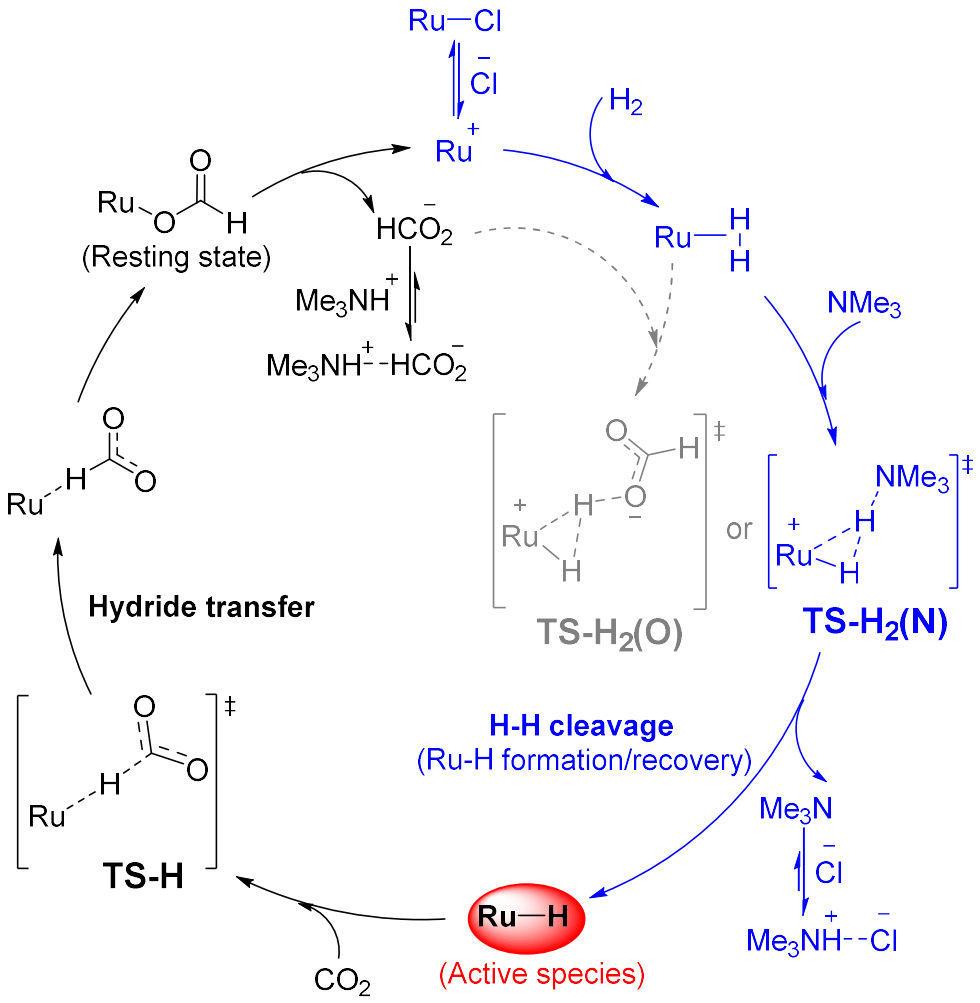

Scheme 1. Proposed mechanism for catalytic hydrogenative CO_2 reduction.

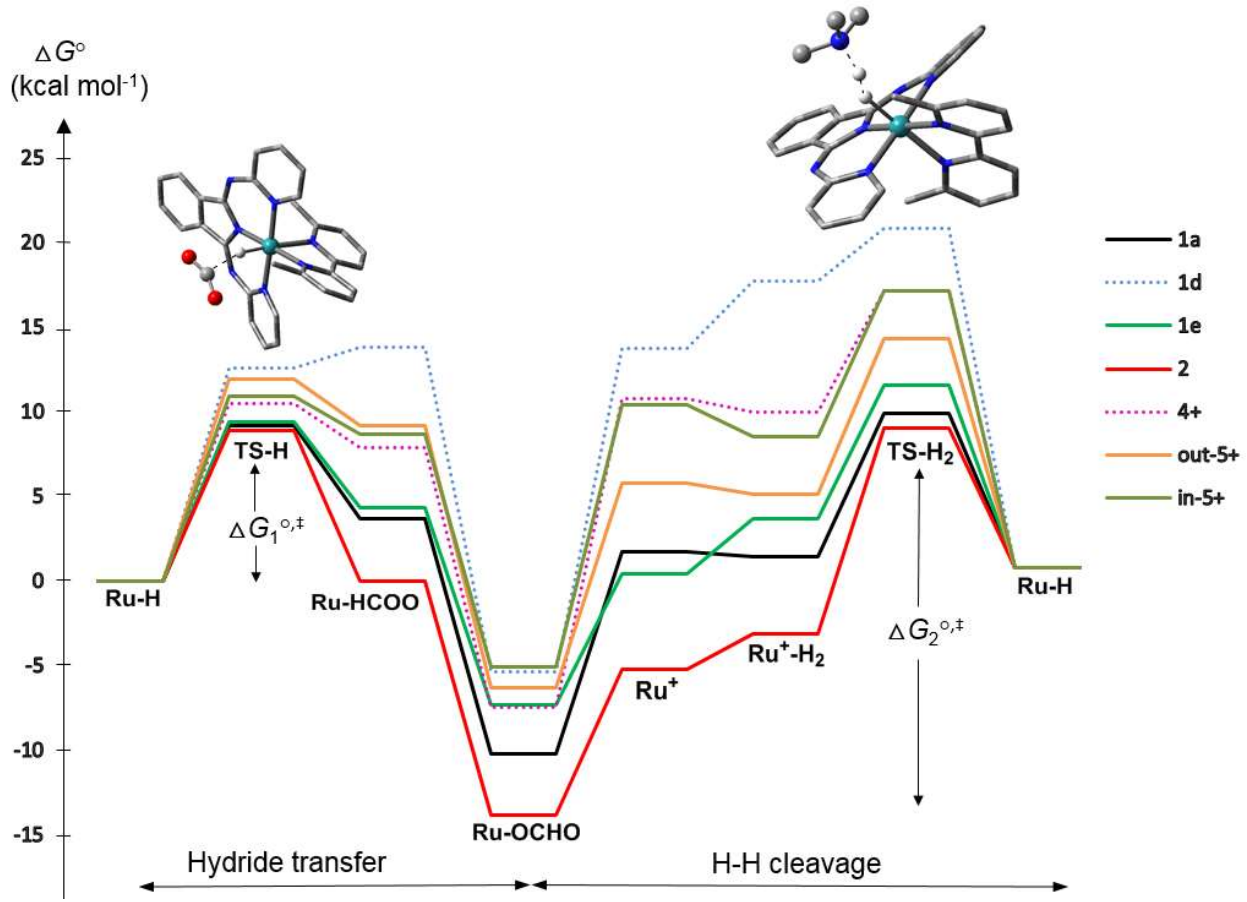

Figure 6. Free energy reaction coordinates for the catalytic cycles of **1a**, **1d**, **1e**, **2**, $\mathbf{4}^{+}$, *in*- and *out*-$\mathbf{5}^{+}$. TS structures for complex **1e** are shown. For clarity, reaction coordinates for **3a** and **3b** are not shown as they almost overlap with that for **1a** (cf. Table 3 and Figure S12).

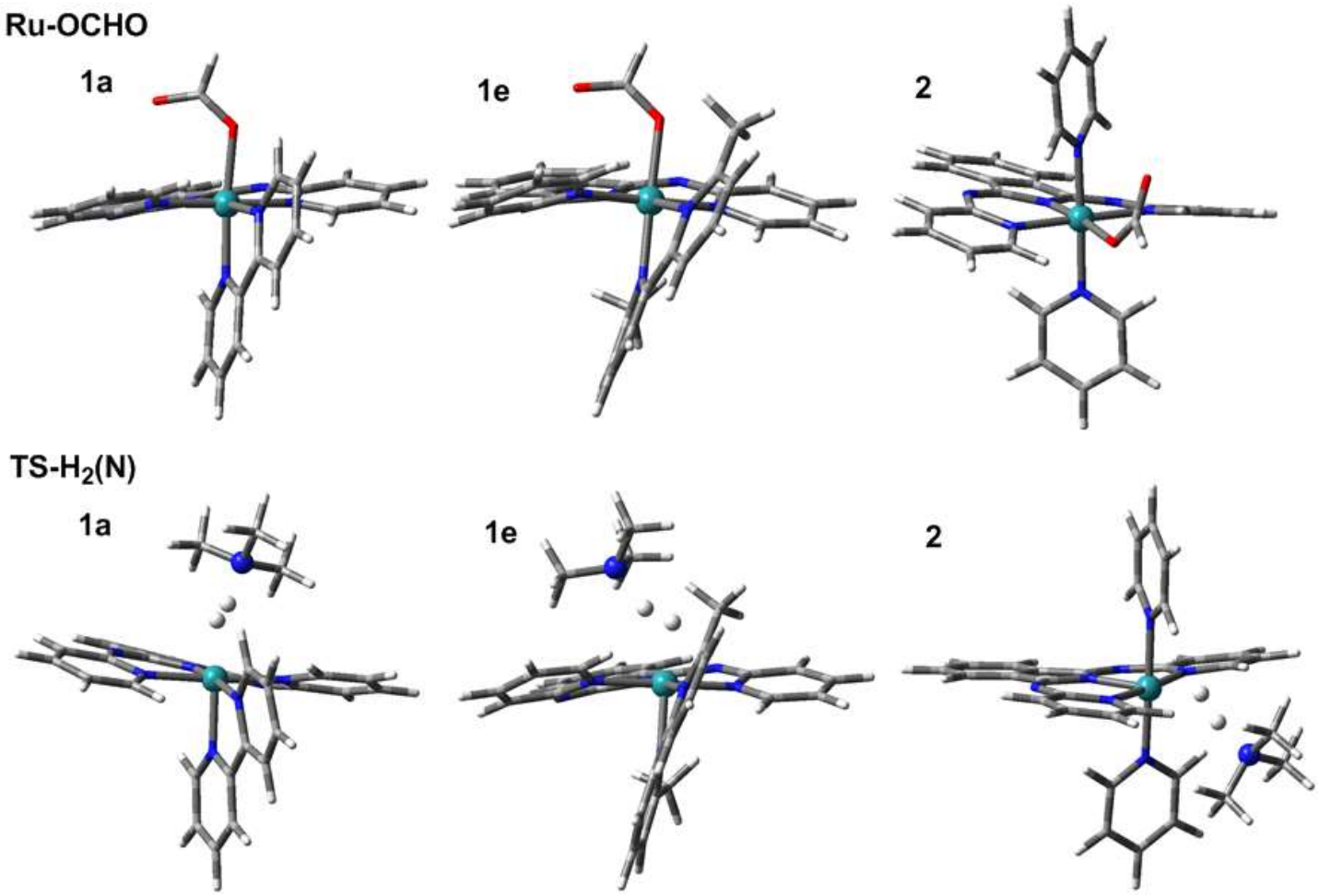

Figure 7. Mercury representation of DFT calculated structures for Ru-OCHO intermediates (top) and TS_2 (bottom) for **1a** (left), **1e** (middle) and **2** (right).

Table 1. Selected XRD metric parameters for **1e**.

Entry	**Complex**	ph-py[a] (90° ideal)	py-py[b] (0° ideal)	H-bond/contact[c]	
1	Ru-Cl, **1e**	58.4	34.7	2.72/3.18/0.98/109.2 2.91/3.18/0.98/97.2	Cl-HC-Me

[a]Angle between the best planes formed by the C atoms of the phenyl ring of *bid*$^-$ and the C,N atoms of the pyridyl ring of *bpy* cis to the Ru-Cl or Ru-O bond.

[b]Angle between the best planes formed by the C and N atoms of the pyridyl rings and of the *bid*$^-$ ligand.

[c]All bond distances in Å and angles in degrees (°). Hydrogen bonding/contacts include Ru-Cl/Ru---H/C-H distances and the RuClH angle.

Table 2. Electrochemical Data and Initial Catalytic Performances of Mononuclear Catalysts for Hydrogenative CO_2 Reduction.

Entry	Tridentate Ligand	Catalysts	$E_{1/2}$ for Ru(III/II)[a]	TOF_i [d]	
	bid$^-$				
1		**1a**	0.30	366.0 (178.4)	Ref [15]
2		**1b**	0.41	415.7 (259.8)	Ref [15]
3		**1c**	0.17	212.2 (132.6)	Ref [15]
4		**1d**	-0.49	0	*Tw*
5		**1e**	0.30	>1140 (>713)[e]	*Tw*
6		**2**	0.29	119.7 (74.8)	*Tw*
	dpb$^-$				
7		**3a**	0.02	192.6 (120.4)	*Tw*
8		**3b**	0.18	211.3 (132.1)	*Tw*
	trpy				
9		**4**$^+$	0.87	1.6 (1.0)	Ref [15]
10		***out*-5**$^+$	0.30[b], (0.63 V)[c]	115.3 (72.1)	*Tw*
11		***in*-5**$^+$	0.43[b], (0.82 V)[c]	59.6 (37.3)	*Tw*

Tw = This work. [a] $E_{1/2}$ (V) obtained from $(E_{p,a} + E_{p,c})/2$ vs SSCE. Scan rate 100 mV/s in glassy carbon working electrode and a Pt disk counter electrode, see supporting information. [b] $E_{1/2}$ values for the deprotonated forms obtained by adding Et_3N to the DCM solution containing the protonated forms of the complex. [c] $E_{1/2}$ values for the protonated forms. [d] TOF_i (h^{-1}): Initial Turnover Frequencies, considering the first 90 minutes. In parenthesis values normalized with regard to complex **4**$^+$. Reaction conditions: 0.3 mM solution of complexes dissolved in a 9:1 mixture of TFE and NEt_3 at 25 bar of CO_2 and 25 bar of H_2 at 100°C. [e] TOF_i was calculated from first 20 min due to fast deactivation of the system (see Figure 4).

Table 3. Computed free energies ($G°_{298}$, kcal mol^{-1}) relative to Ru-H intermediate for all stationary points in the hydrogenative CO_2 reduction catalytic cycle for complexes **1-5**.[a]

Stationary Points[b]	**1a**	**1d**	**1e**	**2**	**3a**	**3b**	**4$^+$**	***out*-5$^+$**[c]	***in*-5$^+$**[c]
Ru-H	0.0	0.0	0.0	0.0	0.0	0.0	0.0	0.0	0.0
TS-H	9.2	12.6	9.4	8.9	9.6	9.7	10.5	11.9	10.9
Ru-HCOO	3.7	13.8	4.3	0.0	4.8	6.1	7.9	9.2	8.7
Ru-OCHO	**-10.2**	**-5.4**	**-7.3**	**-13.8**	**-8.6**	**-7.7**	**-7.5**	**-6.3**	**-5.1**
Ru$^+$	1.7	13.7	0.4	-5.2	3.8	5.6	10.8	5.8	10.4
Ru$^+$-H_2	1.4	17.7	3.7	-3.1	0.1	2.9	10.0	5.1	8.5
TS-H_2(N)	**9.9**	**20.8**	**11.6**	**9.0**	**10.7**	**12.0**	**17.1**	**14.3**	**17.1**
$\Delta G_1^{\circ,\ddagger}$[d]	9.2	12.6	**9.4**	8.9	9.6	9.7	10.5	11.9	10.9
$\Delta G_2^{\circ,\ddagger}$[e]	20.1	26.2	**18.9**	22.8	19.3	19.7	24.6	20.6	22.2

[a] M06-L(SMD=2,2,2-trifluoroethanol)/6-311+G(2df,p)|SDD//M06-L(SMD=2,2,2-trifluoroethanol)/6-31+G(d,p)|6-31G(d)|SDD; for stoichiometric balance, the zero of energy includes Ru-H and one molecule each of H_2, CO_2, and Me_3N; other species have analogous appropriate spectator compounds. [b] See Figure 6. [c] Values shown for lowest energy pyrazole ligand protonation states, which vary for different intermediates (see discussion and SI). [d] Free energy difference between TS-H and Ru-H. [e] Free energy difference between TS-H_2(N) and Ru-OCHO.

TOC